Claudin-8 modulates paracellular permeability to acidic and basic ions in MDCK II cells

Susanne Angelow[1,3], Kwang-Jin Kim[2,3,4] and Alan S. L. Yu[1,3]

Divisions of [1]Nephrology and [2]Pulmonary and Critical Care Medicine, [3]Departments of Medicine and Physiology and Biophysics, and [4]the Will Rogers Institute Pulmonary Research Center, University of Southern California Keck School of Medicine, Los Angeles, CA 90033, USA

Renal net acid excretion requires tubular reabsorption of filtered bicarbonate, followed by secretion of protons and ammonium in the collecting duct, generating steep transtubular gradients for these ions. To prevent passive backleak of these ions, the tight junctions in the collecting duct must be highly impermeable to these ions. We previously generated a Madin-Darby canine kidney (MDCK II) cell line with inducible expression of claudin-8, a tight junction protein expressed in the collecting duct. In these cells, claudin-8 was shown to function as a paracellular barrier to alkali metal and divalent cations. We have now used this model to test the hypothesis that claudin-8 also functions as a paracellular barrier to acidic or basic ions involved in renal acid excretion. We developed a series of precise and unbiased methods, based on a combination of diffusion potential, short-circuit current, and pH stat measurements, to estimate paracellular permeability to protons, ammonium and bicarbonate in MDCK II cells. We found that under control conditions (i.e. in the absence of claudin-8), these cells are highly permeable to the acidic and basic ions tested. Interestingly, proton permeation exhibited an unusually low activation energy similar to that in bulk solution. This suggests that paracellular proton transfer may occur by a Grotthuss mechanism, implying that the paracellular pores are sufficiently wide to accommodate water molecules in a freely mobile state. Induction of claudin-8 expression reduces permeability not only to protons, but also to ammonium and bicarbonate. We conclude that claudin-8 probably functions to limit the passive leak of these three ions via paracellular routes, thereby playing a permissive role in urinary net acid excretion.

(Received 21 September 2005; accepted after revision 24 November 2005; first published online 1 December 2005)
Corresponding author A. S. L. Yu: University of Southern California Keck School of Medicine, Division of Nephrology, 2025 Zonal Avenue, RMR 406, Los Angeles, CA 90033, USA. Email: alanyu@usc.edu

The kidney plays an important role in acid–base balance by regulating urinary net acid excretion. This involves two steps (Hamm, 2004). First, filtered HCO_3^- is reabsorbed, mainly in the proximal tubule and loop of Henle. Second, H^+ and NH_4^+ are actively secreted in the collecting duct. These active, transcellular transport processes generate large transtubular concentration gradients. To prevent passive backleak and dissipation of these gradients, the entire collecting duct, including the tight junctions, must be highly impermeable to these ions. Defects in collecting duct ion permeability can impair acid excretion and cause metabolic acidosis (Batlle & Flores, 1996; Zawadzki, 1998).

The rate-limiting step in paracellular permeability in renal tubular epithelium occurs at the tight junction. Recent studies indicate that a family of transmembrane tight junction proteins known as claudins form paracellular pores (Tsukita & Furuse, 2000; Schneeberger & Lynch, 2004; Van Itallie & Anderson, 2004). Overexpression studies in epithelial cell lines have begun to delineate the permeability properties of individual isoforms (McCarthy *et al.* 2000; Furuse *et al.* 2001; Van Itallie *et al.* 2001, 2003; Amasheh *et al.* 2002; Yu *et al.* 2003; Alexandre *et al.* 2005). Their selectivity is in part determined by charged residues on their first extracellular domain (Colegio *et al.* 2002; Van Itallie *et al.* 2003). By excluding certain solutes, claudins also form the paracellular barrier (Yu *et al.* 2003).

Claudin-8 is expressed at the tight junction of the distal nephron, extending continuously from the early distal convoluted tubule to the tip of the inner medullary collecting duct (Li *et al.*, 2004). We previously generated an MDCK II cell line with inducible expression of claudin-8 and used it to show that claudin-8 acts as an important component in the formation of a significant barrier to monovalent alkali metal cations, divalent cations, and organic cations (Yu *et al.* 2003). Because claudin-8 is normally expressed in the entire collecting duct, we hypothesized that it might also be necessary for the paracellular barrier to H^+, NH_4^+ and/or HCO_3^-, thereby playing a permissive role in renal

 DOI: 10.1113/jphysiol.2005.099135

Table 1. Solutions used for electrophysiological studies in Ussing chamber

	A	B	C	D	E	F	G	H	I	J	K
NaCl	150	—	150	—	—	75	140	140	20	20	10
ChCl	—	120	—	—	—	—	—	—	—	—	—
NH_4Cl	—	—	—	150	—	—	1	10	—	—	—
CsCl	—	—	—	—	150	—	—	—	—	—	—
$NaHCO_3$	—	—	—	—	—	—	—	—	22	2.2	22
$CaCl_2$	2	2	2	2	2	2	2	2	2	2	2
$MgCl_2$	1	1	1	1	1	1	1	1	1	1	1
Glucose	10	10	10	10	10	10	10	10	10	10	10
Hepes-Tris	—	—	10	10	10	10	10	10	10	10	10
pH	7.4	7.4	7.4	7.4	7.4	7.4	7.4	6.4	7.4	6.4	7.4
O_2 (%)	100	100	100	100	100	100	100	100	95	95	95
CO_2 (%)	—	—	—	—	—	—	—	—	5	5	5

Solute concentrations are mM. All solutions were adjusted with mannitol to an osmolarity of ~320 mosmol l^{-1}. ChCl, choline chloride.

acid excretion. In this study, we developed methods to measure paracellular H^+, NH_4^+ and HCO_3^- permeability in control MDCK II cells and investigated how these are affected by claudin-8 induction. Our results reveal a strikingly different mechanism for paracellular H^+ transport compared to other monovalent cations. We further show that claudin-8 also acts as a paracellular barrier to both NH_4^+ and HCO_3^-, consistent with an important role in net acid excretion.

Methods

Cell culture

MDCK II TetOff claudin-8 NFL cells (Yu *et al.* 2003) were maintained in Dulbecco's modified Eagle's medium with 5% fetal bovine serum, and 20 ng ml^{-1} doxycycline for 2 days prior to plating onto 1 cm^2 Snapwell polyester filters (Corning Life Sciences, Corning, NY, USA). To mitigate the potential effects of differential growth rate, cell culture on filters was initiated by plating the cells at twice confluent density (approximately 4×10^5 cm^{-2}) and washing off the excess cells after overnight incubation. The culture medium was exchanged every 3 days. Because doxycycline in solution degraded rapidly, medium containing doxycycline (made from frozen doxycycline stocks) was stored at 4°C in the dark, and used within 7 days. To induce claudin-8 expression, doxycycline was omitted from the culture medium starting from the day of plating (Dox−). In matching control plates, doxycycline was included in the medium to suppress claudin-8 expression (Dox+). All studies were performed after 4–5 days in culture.

Ussing chamber setup

The solutions used are listed in Table 1. Filter inserts containing cell monolayers were gently rinsed two times with unbuffered or buffered saline Ringer solution (solution A or C, respectively), mounted in one of six Ussing chambers and allowed to stabilize for 15–30 min. The reservoir on each side of the monolayer was filled with 4–6 ml fluid and continuously bubbled and stirred with either 100% O_2 or 95% O_2–5% CO_2 (for HCO_3^--buffered solutions) gas lifts. The chambers were warmed (to 37°C, unless otherwise indicated) by a water jacket fed from a circulating water bath. In studies to assess the temperature dependence of permeability, the temperature in the Ussing chamber fluid was directly monitored by immersion of a metal thermocouple probe (Physitemp Instruments, Clifton, NJ, USA) and the water bath temperature adjusted until the solution temperature was 37°C, 24°C, or 16°C. The coefficient of variation in the temperature among the six chambers was 1%.

Voltage-sensing electrodes consisting of Ag–AgCl pellets and current-passing electrodes of Ag wire were connected by agar bridges containing 3 M KCl and interfaced via headstage amplifiers to a microcomputer-controlled voltage/current clamp (DM-MC6 and VCC-MC6, respectively; Physiologic Instruments, San Diego, CA, USA). Voltage-sensing electrodes were matched to within 1 mV asymmetry and corrected by an offset-removal circuit. The fluid resistance was determined in the absence of a filter and electrically compensated using the series compensation circuit on the clamp. The voltage was first measured with blank filters in each combination of solutions to be used for the experiments. The values obtained, which were generally less than 1 mV in magnitude, represent the difference in junction potentials between the two voltage-sensing bridges, summed with any potential that might exist across the blank filter membrane. These were subtracted from all subsequent measurements with filters containing attached cell monolayers to determine transepithelial voltage. The spontaneous potential difference in control MDCK II monolayers was generally less than 0.2 mV and was ignored. Transepithelial voltages reported are

referenced to the apical side. Short circuit current flowing in the basolateral-to-apical direction was considered positive.

The total resistance between apical and basal sides was determined at the start of the experiment from the current evoked by a 5 mV bipolar voltage pulse. The background resistance determined with blank filters was subtracted from the total resistance measured with filters containing attached cell monolayers to determine the transepithelial resistance (TER) and hence conductance (TER^{-1}). NaCl dilution potentials were determined with 150 mM NaCl in one chamber and 75 mM NaCl in the other (solutions C and F, respectively), and used to determine P_{Na} and P_{Cl}. CsCl biionic potentials were determined with 150 mM NaCl in one chamber and 150 mM CsCl in the other (solutions C and E, respectively), from which P_{Cs} could be deduced.

H^+ permeability studies

These studies were performed in unbuffered solution (solution A) so that pH changes could be readily detected. All solutions were bubbled with 100% O_2 for at least 30 min at 37°C to displace dissolved CO_2, and then adjusted to pH 7.4 with NaOH. The HCl diffusion potential is highly dependent on the permeability of the monolayer to other permeant ions, primarily Na^+ for MDCK II cells. Therefore, to maximize the HCl diffusion potential, these measurements were performed in Na^+-free solution containing a reduced concentration of a relatively impermeant monovalent cation, choline (solution B). The concentration of choline chloride was chosen to be 120 mM because at lower concentrations the fluid resistance exceeded the maximum that could be automatically compensated by our voltage clamp.

To generate a steep transmonolayer H^+ concentration gradient, an aliquot of 1 M HCl was added to one side to achieve a final concentration between 0.1 and 1 mM (*cis* compartment, final pH 3–4). This pH range was chosen because, in preliminary experiments, we found very little effect when we acidified to a pH much higher than 4. With the monolayer current-clamped to zero (i.e. open circuit condition), the instantaneous diffusion potential was then recorded. The monolayer was then voltage-clamped to zero to determine the short-circuit current. This current tended to decline rapidly over the initial 1–2 min (Fig. 1), which we attribute to the generation of a localized pH gradient in the unstirred layer, so the peak value was taken to be the true short-circuit current. The pH was continuously monitored in the *trans* compartment using a calomel combination pH microelectrode connected to a pH meter and chart recorder. Despite careful washing of the cell monolayers and equipment to remove all traces of soluble buffers, the rate of pH change was low and appeared to underestimate true net H^+ transport by 5- to 10-fold, indicating the presence of occult buffering, perhaps by the cell membrane glycocalyx. Net H^+ transport was therefore determined by a manual pH stat method. In brief, the pH in the *trans* compartment was maintained within ± 0.2 units of its baseline value by the repeated addition of 6 μl aliquots of 2.5 mM NaOH with a pipettor (Rainin Pipetman P-10, precision ± 0.03 μl). Over the course of a typical 10 min experiment, up to 24 μl were added, contributing less than 0.5% to the total compartment volume. The amount of NaOH added was divided by the duration between time points of pH identity to determine the rate of H^+ appearance in the *trans* compartment. Chambers were washed extensively after each experiment to prevent carryover of trace amounts of acid into subsequent unbuffered solutions.

Ammonium and bicarbonate permeability studies

Biionic potential measurement to estimate the relative ammonium permeability was determined at pH 7.4 with 150 mM Na^+ in one chamber and 150 mM NH_4^+ in the other (solutions C and D). Because the pK_a of NH_3/NH_4^+ is 9.03, 98% of the ammonia is protonated at this pH and only 2% exists as dissolved NH_3. Nevertheless, it is possible for NH_3 to diffuse across the monolayer, thereby dissipating the ammonium gradient and alkalinizing the other side. Therefore, an alternative protocol was also devised in which a 10-fold gradient of NH_4Cl was established by using two solutions in which the pH was adjusted so that their NH_3 concentrations would

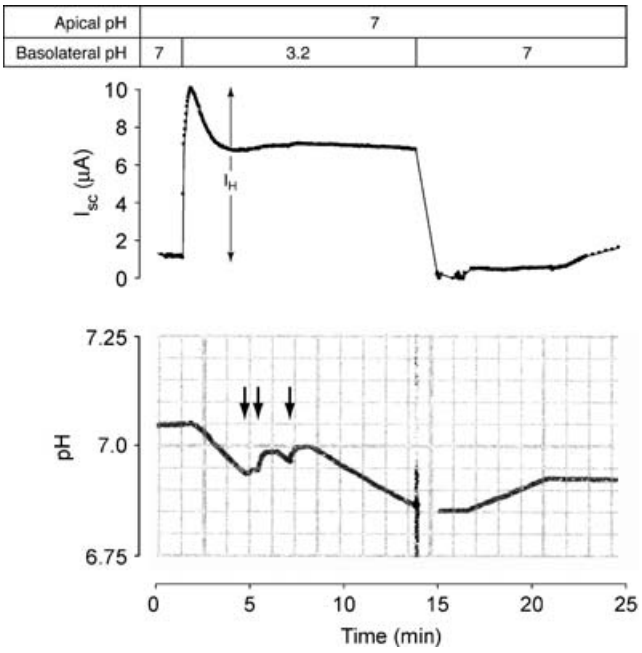

Figure 1. Typical data from a pH gradient experiment
I_{SC}, short-circuit current; pH, apical chamber pH; I_H, short-circuit current attributable to transepithelial pH gradient. Arrows indicate time points at which NaOH was added to the apical chamber.

be identical (solution G, 1 mM NH_4Cl at pH 7.4, and solution H, 10 mM NH_4Cl at pH 6.4). We then measured the NH_4Cl dilution potential and short-circuit current. Although in this protocol there is a modest transmonolayer pH gradient (from pH 6.4–7.4), we have established in our H^+ permeability studies that this gradient itself is insufficient to induce a significant diffusion potential or short-circuit current due to free H^+ (see above).

Bicarbonate permeability was estimated from the dilution potential generated by a 10-fold $NaHCO_3$ gradient (solutions I and J) in the presence of a constant partial pressure of CO_2. Again, there is a small pH gradient from 6.4 to 7.4 that would not be expected to influence the results. The NaCl dilution potential was determined in the same monolayers using 20 and 10 mM NaCl in bicarbonate-containing solution (solutions I and K).

Mathematical and statistical analysis

The relative ionic permeabilities of the monolayers were calculated from dilution or biionic potentials using the Goldman-Hodgkin-Katz (GHK) voltage equation (Hille, 2001). We have previously shown that the GHK equation fits the behaviour of paracellular cation permeation in MDCK II cells reasonably well (Yu *et al.* 2003). The contributions of Ca^{2+}, Mg^{2+}, Tris and Hepes were ignored because they were present at low concentrations and their permeability was assumed to be low. In experiments with three permeant ions ($Na^+/Cl^-/HCO_3^-$, and $Na^+/Cl^-/NH_4^+$), two dilution potentials were determined (NaCl, and either $NaHCO_3$ or NH_4Cl). A GHK equation was written for each and solved to derive the relative permeabilities. The absolute permeability to Na^+ was determined by the method of Kimizuka & Koketsu (1964) using the equation

$$P_{\mathrm{Na}} = \frac{RT}{F^2} \frac{G}{[\mathrm{Na}^+] + \frac{P_{\mathrm{Cl}}}{P_{\mathrm{Na}}}[\mathrm{Cl}^-] + \frac{P_{\mathrm{HCO_3}}}{P_{\mathrm{Na}}}[\mathrm{HCO_3}^-] + \frac{P_{\mathrm{NH_4}}}{P_{\mathrm{Na}}}[\mathrm{NH_4}^+]}$$

where G is the overall monolayer conductance per unit surface area, T is the absolute temperature, R is the gas constant and F is Faraday's constant. From the value of P_{Na}, and the known relative permeabilities to the other ions, the absolute permeabilities to those ions could then be deduced.

Net monovalent cation (H^+ or NH_4^+) flux, J, across a monolayer of surface area, A, was calculated from the peak short-circuit current, I_{SC}. Since the Cl^- concentration difference was very small, and the Cl^- permeability very low (Table 2), its contribution to the current was ignored, and H^+ or NH_4^+ was assumed to be the sole charge carrier. From the concentration difference between apical and basolateral baths, ΔC, the permeability, P, could then be derived:

$$J = \frac{I_{\mathrm{SC}}}{FA} \qquad P = \frac{J}{\Delta C}$$

In all calculations, activities rather than concentrations were used. The mean activity coefficient of each monovalent salt was assumed to be the same as that of NaCl, and the anion and cation in each case were assumed to have the same activity coefficient (Guggenheim assumption).

Data (except in Fig. 7) are presented as means ± S.E.M. (n) for a single experiment, where n indicates the number of monolayers used. Differences between the means of two groups were assessed for statistical significance using Student's unpaired two-tailed t test, where appropriate. The ratio of permeabilities under Dox− and Dox+ conditions (Fig. 7) was estimated by the ratio of the means of the permeabilities under these two conditions. Approximate values for the 95% confidence intervals of this estimator were determined by the Taylor series method (Dann & Koch, 2005). Differences in the estimated permeability ratio of different cations were considered to be statistically significant ($P < 0.05$) if their 95% confidence intervals did not overlap. Non-linear regression analysis of Arrhenius plots (Fig. 8) was performed by the Levenberg-Marquardt method using GraphPad Prism 3 software. The best-fit value for the slope of the line in each experimental group was determined independently. This was then compared with a global fit in which one shared best-fit value for all the groups was selected, and an F test performed to assess for statistically significant differences between the groups.

Table 2. Ionic permeability of MDCK II cells expressing claudin-8

	Mean diameter (Å)*	Relative mobility†	Permeability ($\times 10^{-6}$ cm s^{-1})	
			Dox+	Dox−
H^+	0.5	6.45	137.4 ± 4.6	97.5 ± 0.6
Na^+	1.9	1.00	62.4 ± 3.5	27.9 ± 0.6
Cs^+	3.38	1.71	47.4 ± 3.2	21.0 ± 0.3
NH_4^+	2.96	1.44	61.3 ± 3.1	28.7 ± 0.6
Cl^-	3.62	1.50	2.8 ± 0.2	3.1 ± 0.5
HCO_3^-	4.1	0.89	14.4 ± 0.9	6.5 ± 0.9

* The mean diameter of the alkali metal cations was defined as twice the Pauling radius of the non-hydrated ion (Robinson & Stokes, 1959). The mean diameter of H^+ was estimated from the Slater atomic radius (Slater, 1964). The mean diameter of HCO_3^-, derived from Fig. 3 in Halm & Frizzell (1992), was defined as the geometric mean of the dimensions of a rectangular box that would contain the ion as determined using Corey-Pauling-Koltum space-filling molecular models. † Relative free solution mobility of each ion was calculated from the ratio of its limiting equivalent conductivity to the limiting equivalent conductivity of Na^+, both at 35°C (Robinson & Stokes, 1959) or, in the case of HCO_3^-, at 25°C (Lide, 2002).

Results

Development of methods to estimate passive transepithelial H^+ permeability

To determine the passive H^+ permeability of the epithelial monolayer, a transepithelial pH gradient was imposed by equilibrating the cells in an Ussing chamber filled on both apical and basolateral sides with an identical unbuffered solution at pH 7, then rapidly acidifying the solution in one reservoir (*cis* side) to pH 3–4 while monitoring the pH continuously in the other reservoir (*trans* side). The permeability was then estimated by three different methods. First, in zero current-clamp mode, an instantaneous diffusion potential was measured (*trans* positive). Second, in zero voltage-clamp mode, a short-circuit current (flowing from *cis* to *trans*) was measured (Fig. 1). As the Cl^- concentration difference was negligible (0.1–1 mM), the Cl^- permeability is known to be low (Yu *et al.* 2003), and all other ion concentrations were equal on either side of the monolayer, the short-circuit current (I_{SC}) was assumed to represent H^+ movement down its concentration gradient. This peaked almost immediately, then relaxed to a lower steady-state value, reflecting the establishment of unstirred layers, as well as a time-dependent acidification-induced increase in transepithelial resistance (not shown) of unclear aetiology. Third, also in zero voltage-clamp mode, the pH in unbuffered solution on the *trans* side was continuously monitored as it began to acidify, and was titrated with aliquots of NaOH by the pH stat method (Fig. 1).

From measurements taken by each of the three methods (Fig. 2*A*), an estimate of the absolute transepithelial H^+ permeability was calculated (see Methods for assumptions used in these calculations). All three estimates were similar in magnitude, suggesting that our assumptions were reasonable and basically correct (Fig. 2*B*). However, data obtained by the diffusion potential method had much higher variance, and tended to bias toward higher values, while the pH stat method tended towards slightly lower values than I_{SC}. In general, steady-state measurements of permeability (i.e. diffusion potentials) tend to overestimate dynamic measurements (i.e. short-circuit currents or conductances), presumably due to the presence of strong cation-binding sites in the paracellular pore, as we have shown previously for small alkali metal cations (Yu *et al.* 2003). Permeability by pH stat measurement (which took several minutes) tended to underestimate the permeability by I_{SC} measurement (which was almost instantaneous). This is likely because the pH stat measurement occurred over a period of time when local pH gradients within the unstirred layers may have reached a steady state which would retard net H^+ flux. Furthermore, the acidification of the basolateral medium induced a rise in TER over a time course of several minutes, a phenomenon which has been explained by titration of negative charges lining the paracellular pore which leads to a decrease in cation permeability (Cereijido *et al.* 1978). The good correlation of data obtained by pH stat measurements with results derived from the diffusion potential and the peak I_{SC} show, however, that the increase

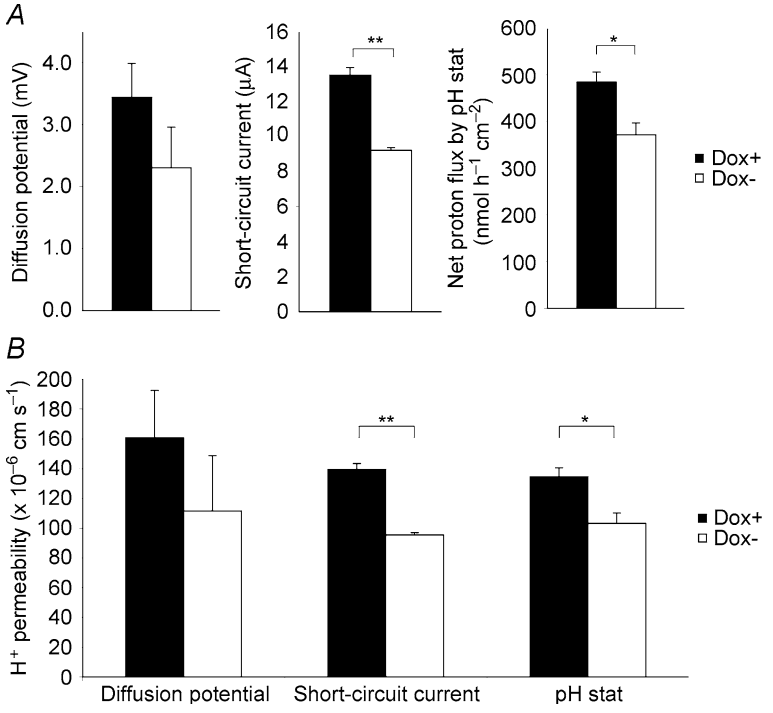

Figure 2. Determination of passive, transepithelial H^+ permeability by three independent methods
A, HCl diffusion potential, short-circuit current, and pH stat-titrated net proton flux measured after imposing a 10^4-fold transepithelial H^+ gradient, in claudin-8-induced (Dox−) and uninduced (Dox+) MDCK II cells. *B*, comparison of the H^+ permeability determined by the three methods. Columns in *A* and *B* represent mean ± S.E.M. ($n = 3$). $^*P < 0.05$; $^{**}P < 0.00005$.

in TER and thus changes in transepithelial permeability by acidification cannot significantly influence the monolayer's permeability to protons. In subsequent studies, peak I_{SC} measurement was used as the primary method to determine H^+ permeability because this method was more precise than determination of the diffusion potential, was experimentally easier than pH stat measurements, and appeared to be the least biased of the three methods.

Effect of claudin-8 on paracellular H^+ permeability

The transepithelial permeability of control MDCK II cells to H^+ was found to be 2.2 times that of Na^+, whereas its free solution mobility is more than 6-fold greater than that of Na^+ (Table 2). Claudin-8 expression, induced by culturing the cells in the absence of doxycycline, caused a reduction in the peak short-circuit current and the net H^+ flux estimated by pH stat (Fig. 2*A*). A similar trend was observed in the diffusion potential, but the difference was not statistically significant, probably due to the greater variance in this data set. Interestingly, the calculated claudin-8-induced reduction in H^+ permeability (Figs 2*B* and 7) appeared to be less than the reduction in Na^+ permeability. To test whether doxycycline has any direct influence on permeability which is not related to claudin-8-mediated effects we measured the TER and H^+ permeability of MDCK II TetOff cells (not transfected with claudin-8) which had been cultured in the presence and absence of doxycycline. We could not detect any differences.

MDCK II cells form leaky monolayers in which the major conductive transepithelial pathway is known to be paracellular (Cereijido, 1984). We therefore hypothesized that the transepithelial H^+ permeability that we measured was predominantly paracellular. Paracellular conductance is generally symmetrical, indicating the presence of a single resistance barrier, whereas transcellular conductance through two resistance barriers in series is asymmetrical, except in the specific case where apical and basolateral membrane permeabilities are identical. To distinguish transcellular from paracellular H^+ flux, H^+ permeabilities determined when the H^+ gradient was imposed in the apical-to-basolateral or basolateral-to-apical direction were compared. As shown in Fig. 3*A*, transepithelial H^+ permeability is symmetrical. Furthermore, paracellular conductance is generally non-saturable with increasing concentrations of the transported ion in the physiological range, whereas many transcellular transport processes exhibit saturation. The observed I_{SC} was found to be linearly dependent on the H^+ concentration gradient with no evidence of saturation up to 10^{-3} M (Fig. 3*B*).

If there is a significant transcellular component to the H^+ transport, this could potentially be mediated by either one or both of two known passive transmembrane H^+ transport mechanisms: (1) Na^+–H^+ exchange, which can be inhibited by high concentrations of amiloride, and (2) voltage-gated proton channels, which are generally inhibited by Zn^{2+} (Decoursey, 2003). In initial experiments, 1 mM amiloride was added to both apical and basolateral reservoirs. There was no effect on I_{SC}, yet the rate of acidification in the *trans* side was blunted (Fig. 4, left panel). This is likely because amiloride, a weak base (pK_a 8.7), buffers acid appearing in the *trans* reservoir. To test this, amiloride was added only to the *cis* reservoir (i.e. to the apical side with an apical-to-basolateral H^+ gradient, and to the basolateral side with a basolateral-to-apical gradient). In this setting, the rate of acidification was no longer affected by amiloride (Fig. 4, middle and right panels), confirming that the previous finding was due to amiloride buffering. A similar protocol was necessary for $ZnCl_2$ because of its acidifying effect in unbuffered solution. *Cis* addition of 100 μM $ZnCl_2$ had no effect at all on either I_{SC} or the rate of *trans* acidification when added apically, and only

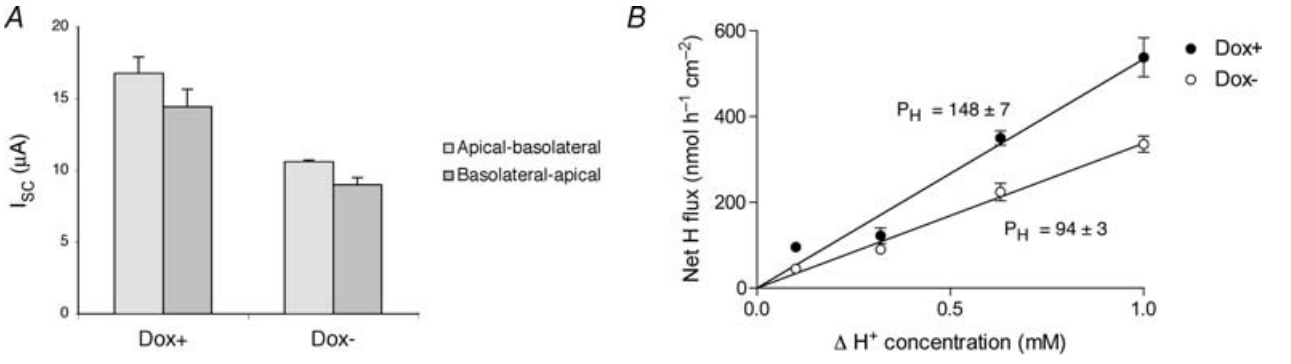

Figure 3. Properties of the H^+ short-circuit current (I_{SC})
A, magnitude of I_{SC} is similar when the H^+ gradient is imposed in different directions. *B*, net H^+ flux (J), calculated from I_{SC}, is proportional to the H^+ concentration difference ($\Delta[H^+]$). Lines were fitted by linear regression to the equation, $J = P \times \Delta[H^+]$. The indicated estimates for the permeability P_H ($\times 10^{-6}$ cm s^{-1}) were derived from the slopes.

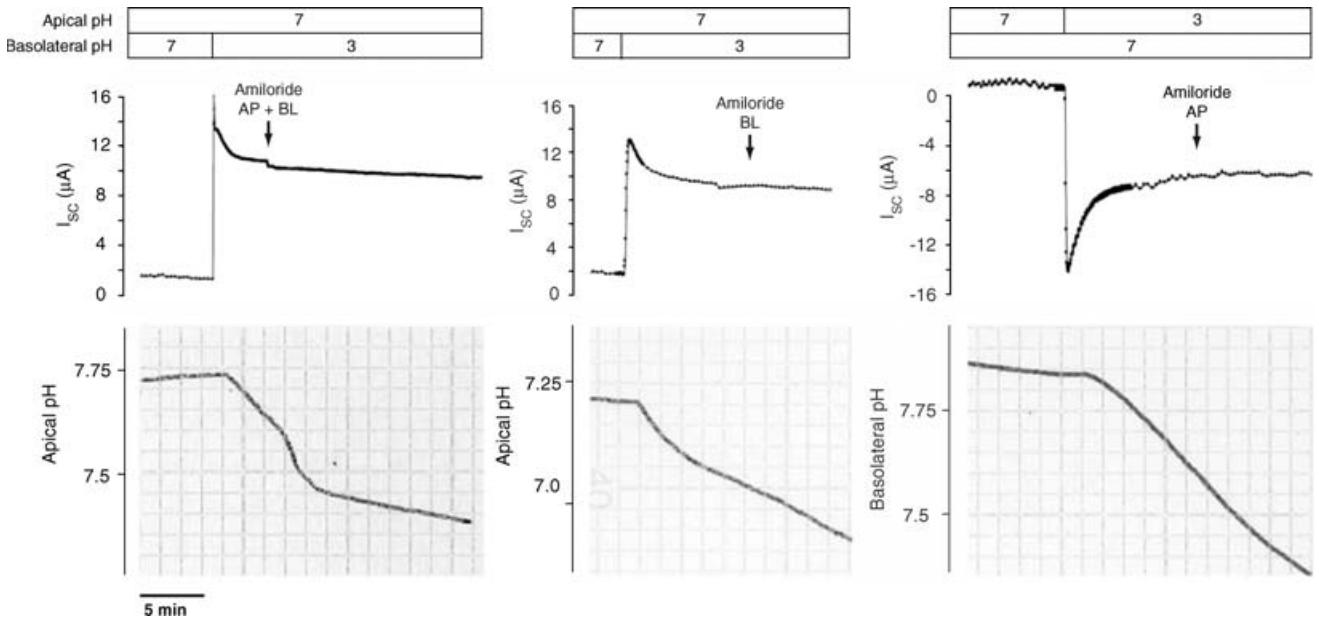

Figure 4. Effect of amiloride in H^+ gradient experiment
The *cis* compartment was acidified, and I_{SC} (positive values indicate current flow from basolateral to apical side) and pH in the *trans* compartment were monitored. Amiloride (1 mM) was then added (arrows), either to the apical chamber (AP), basolateral chamber (BL), or to both (AP + BL).

a small inhibitory effect on I_{SC} when added basolaterally (Fig. 5). These findings confirm that the H^+ permeability we are measuring, and which is decreased by claudin-8 expression, is predominantly via the paracellular pathway.

Effect of claudin-8 on bicarbonate and ammonium permeability

Apart from free H^+, other quantitatively more significant components that contribute to urinary net acid excretion include HCO_3^- and NH_4^+. NH_4^+ permeability was determined from the biionic potential generated by replacing 150 mM Na^+ with equimolar NH_4^+ in the basolateral fluid (Table 2 and Fig. 6*A*). As had been shown for other monovalent cations, induction of claudin-8 in MDCK II by removal of doxycycline caused a significant reduction in NH_4^+ permeability. In this protocol, there is also a gradient of NH_3 across the monolayer that could potentially cause significant transmonolayer NH_3 diffusion and pH changes. An alternative protocol was

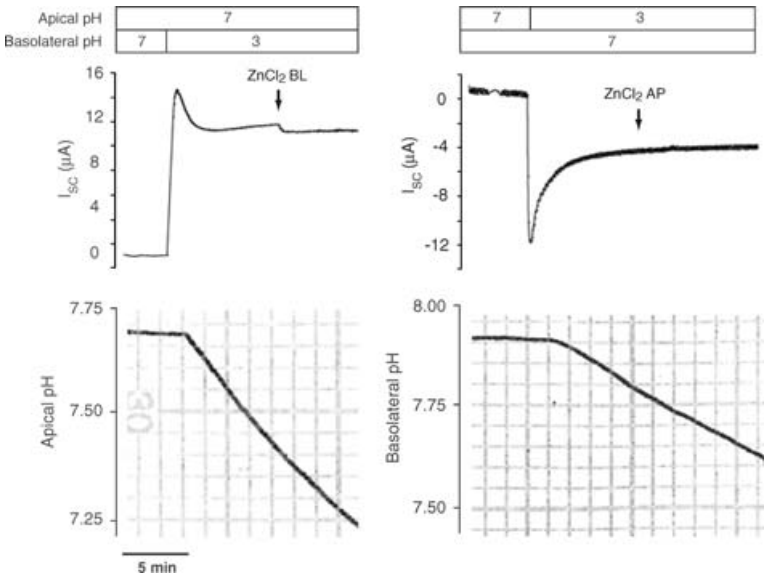

Figure 5. Effect of $ZnCl_2$ in H^+ gradient experiment
The *cis* compartment was acidified, and I_{SC} and pH in the *trans* compartment monitored. $ZnCl_2$ (1 mM) was then added (arrows) to the *cis* compartment (AP, apical; BL, basolateral).

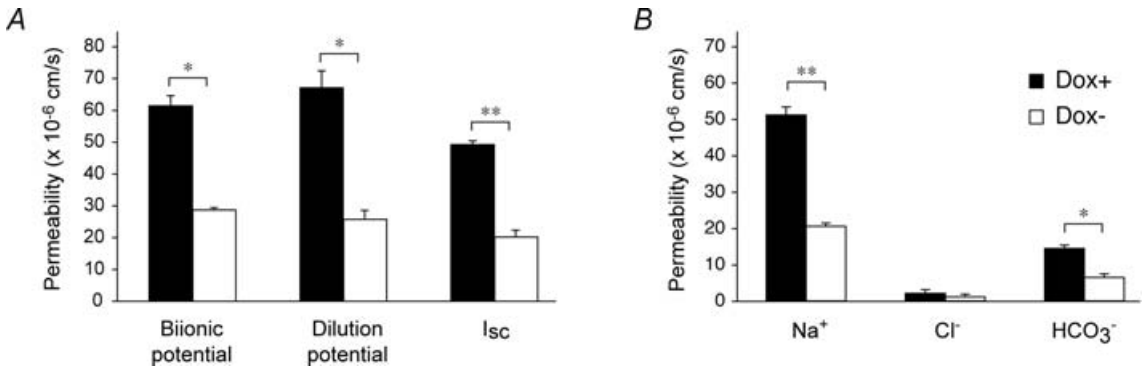

Figure 6. Effect of induction of claudin-8 expression on HCO_3^- and NH_4^+ permeability
A, determination of NH_4^+ permeability by three different methods. *B*, determination of HCO_3^- permeability, concurrently with Na^+ and Cl^- permeability, by dilution potential. $^*P < 0.005$; $^{**}P < 0.0005$ ($n = 4$).

therefore devised in which the NH_4Cl was included at different concentrations on each side, with the pH adjusted so that the NH_3 concentration would be symmetrical. In this situation, an NH_4Cl dilution potential and a short-circuit current, presumed to be mainly carried by NH_4^+, could be measured (Fig. 6*A*). These measurements yielded almost identical NH_4^+ permeabilities to those estimated from the biionic potential data, indicating that NH_3 diffusion does not contribute appreciably to the observed NH_4^+ permeabilities.

HCO_3^- permeability was determined by $NaHCO_3$ dilution potential measurement. Surprisingly, HCO_3^- permeability in control MDCK II cells was substantially higher than Cl^- permeability. Unlike with Cl^-, claudin-8 significantly reduced HCO_3^- permeability (Table 2 and Fig. 6*B*). In control experiments, we added 200 μM 4,4′-diisothiocyanatostilbene-2,2′-disulphonic acid (DIDS) and 1 mM amiloride to inhibit Cl^-–HCO_3^- and Na^+–H^+ exchangers, respectively, transport proteins that are known to participate in transcellular HCO_3^- transport. In the presence of these inhibitors, claudin-8 also decreased HCO_3^- permeability to about 50% of the values measured in uninduced cells treated with doxycycline (data not shown). This result indicates that claudin-8 limits paracellular HCO_3^- diffusion, though we cannot exclude transcellular contributions that are not blocked by the applied inhibitors.

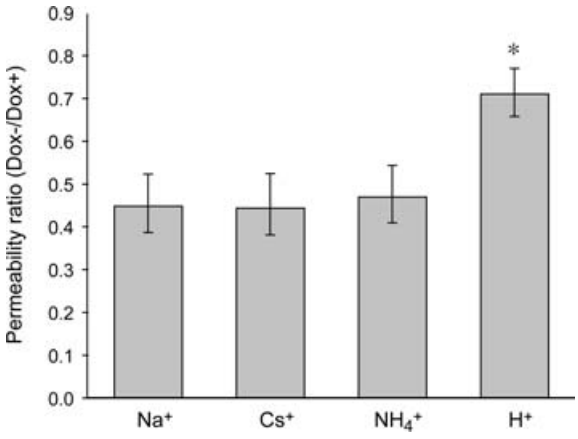

Figure 7. Effect of claudin-8 induction on permeabilities to various cations
Comparison of the effect of claudin-8 induction on permeabilities to various cations, expressed as the ratio of the mean permeability in Dox− (induced) cells to the mean permeability in Dox+ (control) cells. Error bars represent 95% confidence intervals. $^*P < 0.05$ *versus* Na^+, Cs^+ and NH_4^+. Data are representative of three independent experiments.

Temperature dependence of H^+ permeability

In a previous study, we showed that claudin-8 reduced permeability to monovalent alkali metal cations, monovalent organic cations, and divalent cations, all to the same extent (Yu *et al.* 2003). We proposed that these cations all permeated by the same mechanism through claudin-2, a known paracellular cation pore (Furuse *et al.* 2001; Amasheh *et al.* 2002). We further suggested that claudin-8 acts as a cation barrier. When overexpressed, it replaced claudin-2 at the tight junction to reduce permeability to these cations. Thus, we compared the relative reduction in permeability to H^+ and NH_4^+ with that of Na^+ and another alkali metal cation, Cs^+ (Fig. 7). We found induction of claudin-8 reduced NH_4^+ permeability to the same extent as the metal cations (approximately 55%). However, the change in permeability to H^+ upon induction of claudin-8 was consistently less (25–30%), suggesting that the mechanism of paracellular H^+ permeation is distinctly different from that of all the other cations.

To test the latter hypothesis, we measured permeabilities at different temperatures and estimated the activation energy for ion permeation from Arrhenius plots (Fig. 8). Consistent with our previous observations (Yu *et al.* 2003), the activation energy for permeation of Na^+ (23.9 ± 2.8 kJ mol^{-1}) and Cs^+ (29.2 ± 3.3 kJ mol^{-1}) was similar, and did not change upon induction of claudin-8.

However, the activation energy of permeation for H^+ was remarkably low in Dox+ cells (10.6 ± 1.3 kJ mol^{-1}), but increased to the same level as the other cations in Dox− cells with induction of claudin-8 (21.0 ± 1.6 kJ mol^{-1}). These findings indicate that H^+ normally permeates paracellularly through a distinct mechanism with a low activation energy, that appears to be impeded by claudin-8 induction.

Discussion

We have developed reliable electrophysiological methods to assess passive H^+, NH_4^+, and HCO_3^- permeability in MDCK II cells. Where possible, we have tried to corroborate our findings by using several different techniques. In the case of H^+, we are confident that we are measuring paracellular permeability because the H^+ transport profile is symmetrically reversible, non-saturable, and not inhibited by amiloride or Zn^{2+}. Similarly, the paracellular component of transepithelial HCO_3^- permeability was measured by inhibiting trans-cellular transport with amiloride and DIDS.

Mechanism of paracellular H^+ permeation and insights into paracellular pore structure

One of the most surprising findings of this study is that the activation energy for paracellular proton permeation in control MDCK II cells is quite low (~11 kJ mol^{-1}). In bulk aqueous solution, H^+ is known to diffuse rapidly and easily with an activation energy of approximately 11 kJ mol^{-1} (Chernyshev & Cukierman, 2002) and a free solution mobility that is more than 6-fold greater than that of Na^+ (Robinson & Stokes, 1959). The mechanism for bulk solution proton transfer is thought to be a two-step hop and turn process known as the Grotthuss mechanism (Decoursey, 2003). According to this model, proton binding to one side of a water molecule releases a proton from the far side of the molecule that 'hops' onto an adjacent water molecule. This is propagated along a chain of hydrogen-bonded water molecules causing the proton to be transferred across the entire water chain. Each hop is accompanied by a 'turn' or reorientation of the water molecules, as well as a reorganization of the hydrogen-bonded network. In bulk solution, the turn step appears to be activationless, and the rate-limiting

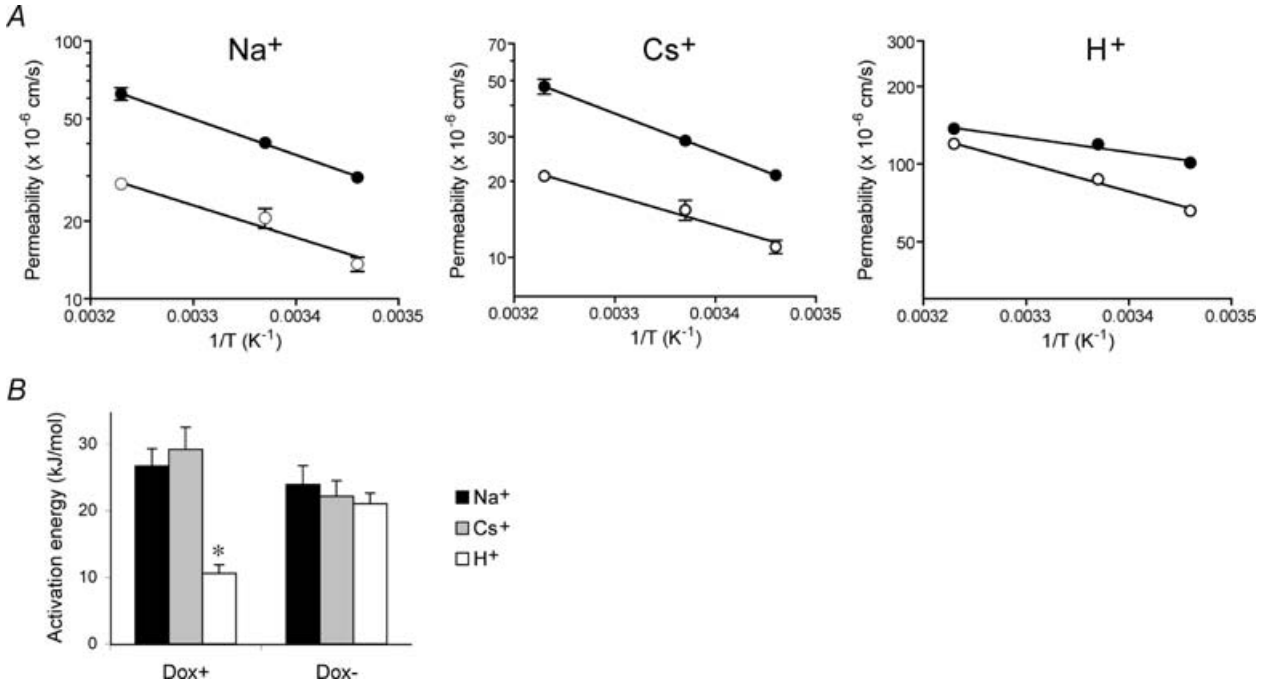

Figure 8. Temperature dependence of paracellular cation permeability
A, Arrhenius plots from Dox+ (●) and Dox− (○) monolayers. The ordinate represents permeability to Na^+, Cs^+ and H^+ on a logarithmic scale. The abscissa represents the reciprocal of the absolute temperature. Data points represent measurements performed at (from left to right) 37°C, 24°C and 16°C. All three plots are scaled to the same proportions so that the slopes of the lines can be directly compared. The lines were obtained by fitting the data by non-linear regression to the equation: $\ln(y) = \ln(K) - E_a/RT$, where y is the ordinate variable, K is a pre-exponential constant, and E_a is the activation energy ($n = 3$). *B*, estimates of activation energy, derived from the slopes of the lines in *A*. $^*P < 0.0005$ for H^+ (Dox+) *versus* H^+ (Dox−), and for H^+ (Dox+) *versus* Na^+ (Dox+).

step is most likely the reorganization of the hydrogen bonds.

All of the known biological channels that permeate protons have much higher activation energies for proton transport than in bulk solution. This is presumably because these channels are sufficiently narrow for water molecules to be constrained in their mobility within the pore (Chernyshev & Cukierman, 2002; Decoursey, 2003). Molecular dynamics simulations demonstrate that proton permeation tends to be slow in channels between 5 Å and 10 Å in diameter (Brewer *et al.* 2001). However, even narrower channels paradoxically exhibit an order of magnitude higher proton permeation rate. This is thought to be because the water molecules in a pore of this size are constrained into a single-file chain known as a water wire, that allows protons to rapidly hop from one water molecule to another. Gramicidin A, which has a pore diameter of 4 Å (Ketchem *et al.* 1997) is the prototype of such a channel. Nevertheless even in gramicidin A channels, the activation energies for proton permeation ($\sim$20 kJ mol^{-1}) are double their values in free solution (Chernyshev & Cukierman, 2002). In channels without water wires, protons are thought to be conducted along a hydrogen-bond chain consisting of the protonatable side chains of amino acid residues lining the pore. In such channels, activation energies for proton permeation are well in excess of 40 kJ mol^{-1} (Decoursey, 2003).

The activation energy for proton permeation that we have found for the paracellular pore of MDCK II cells is lower than in any other known biological ion pore. Furthermore, it is identical to the activation energy of proton transfer in bulk solution. This strongly suggests that protons permeate the paracellular pore by a Grotthuss mechanism analogous to that in bulk solution. For this to occur, the pore must be wide enough for water molecules within it to exhibit the same mobility as in free solution, so that the reorientation of water molecules is not rate-limiting in proton transfer. Simulations of cylindrical pores suggest that for such unrestrained water mobility the pore diameter must be considerably wider than the diameter of a single water molecule (Sansom *et al.* 1996). Estimates of the effective paracellular pore size in MDCK II cells vary, and probably depend on the solute and population of pores under study. Studies of permeability to organic cations suggest a pore diameter in the 7 Å range (Tang & Goodenough, 2003; Yu *et al.* 2003), but such analyses do not account for the contribution of hydration shells and the known electrostatic interaction of cations to the pore wall. Quantitative analyses using neutral polar solutes have yielded estimates for the pore diameter of around 12 Å (Adson *et al.* 1994), which might be consistent with our model for H^+ permeation.

Effect of claudin-8 on H^+, NH_4^+ and HCO_3^- permeability

We found that the induction of claudin-8 expression in MDCK II cells reduces permeability to H^+, NH_4^+ and HCO_3^-. The effect on NH_4^+ permeability may be easiest to explain mechanistically. We previously reported that claudin-8 induction led to a reduction in paracellular permeability to all alkali metal cations to the same extent (Yu *et al.* 2003). Analysing endogenously expressed claudins by a wide range of antibodies we found that a decrease in cation permeability by induction of claudin-8 was associated with a proportionate reduction in expression of the cation-permeating claudin-2. Reduced cation permeability occurred without any change in activation energy in this study. We therefore concluded that claudin-8 is impermeable to metal cations and that replacement of cation-permeable claudin-2 by cation-impermeable claudin-8 could explain these findings. NH_4^+ exhibits similar behaviour to the monovalent alkali metal cations, and has a non-hydrated diameter (2.96 Å) that is virtually identical to that of Rb^+. Thus, our finding that NH_4^+ permeability is reduced to the same extent as Na^+ and Cs^+ (Fig. 7) is consistent with a model in which claudin-2 is NH_4^+ permeable, and is replaced by claudin-8, which acts as an NH_4^+ barrier. Although our data suggest that claudin-2-based pores mediate the paracellular flux of cations in MDCK II we cannot exclude the possibility that other endogenously expressed claudin isoforms, which have not yet been detected in MDCK II cells, could be regulated by claudin-8 expression and contribute to observed changes in permeability.

Although H^+ is also a monovalent cation, its much lower activation energy of paracellular permeation in control MDCK II cells clearly indicates that its mechanism of permeation is quite different from that of NH_4^+ or the alkali metal cations. Also, unlike its effect on the other cations, claudin-8 causes only a modest reduction in H^+ permeability that is associated with a striking increase in the activation energy (Fig. 8). We postulate the existence of a population of paracellular pores which are of sufficient width to accommodate freely mobile water molecules and allow rapid proton permeation by the Grotthuss mechanism. Whether this is a pore constituted by a claudin or other tight junction membrane proteins, or perhaps macroscopic gaps in the tight junction barrier (Sasaki *et al.* 2003), is unknown. In this model, claudin-8 would directly impede H^+ permeation through such a route, for example by filling in gaps.

The effect of claudin-8 on HCO_3^- permeation is not easily explainable. MDCK II cells are intrinsically virtually impermeable to Cl^-, as well as to other halide anions (authors' unpublished results). Claudin-8 does not affect the very small permeability to halide anions

in MDCK II cells, suggesting that it is probably an anion barrier as well as a cation barrier. We find that control MDCK II cell monoalayers have an anomalously high intrinsic permeability to HCO_3^-. Indeed they are 5 times more permeable to HCO_3^- than to Cl^-, even though the non-hydrated HCO_3^- ion is actually larger than Cl^- and the hydrated ion has a lower free solution mobility (Table 2). This suggests the existence of HCO_3^--permeable endogenous claudin isoform(s) in these cells. If claudin-8 is impermeable to HCO_3^-, then induction of claudin-8 might reduce HCO_3^- permeability by replacing a HCO_3^--permeable claudin isoform with a HCO_3^--impermeable one. Further studies will be necessary to test such a model.

Implications for renal net acid excretion

Urinary net acid excretion is equal to the sum of free H^+ (usually quantitatively negligible), NH_4^+, and titratable acidity, minus any urinary HCO_3^- (Hamm, 2004). Filtered HCO_3^- is actively reabsorbed, primarily in the proximal tubule and thick ascending limb, H^+ is actively secreted in the collecting duct where it traps NH_3 secreted by non-ionic diffusion, and NH_4^+ itself may also be directly secreted in this segment. Thus, by the time the tubular fluid reaches the papilla, large transtubular concentration gradients for each of these ions have been established. Luminal pH can generally be lowered to 4.5–5.0 under acid-loading conditions, NH_4^+ concentration can reach as high as 70 mM, and HCO_3^- is less than 0.5 mM (Graber *et al.* 1981; Good *et al.* 1987), whereas basolateral pH is 7.4 with about 2 mM NH_4^+ and 24 mM HCO_3^- (Good *et al.* 1987). Paracellular permeability must be low to prevent backflux of these ions. In fact NH_4^+ permeability in the collecting duct has been measured and is in the range of 10^{-5} cm s^{-1} (Flessner *et al.* 1991), consistent with the existence of a paracellular NH_4^+ barrier. While backflux of H^+ into the interstitium and consequent reduction of free H^+ excretion would not by itself substantially affect net acid excretion, the increase in luminal pH would increase luminal NH_3, and reduce non-ionic diffusion of NH_3, thereby impairing net NH_4^+ secretion. Thus, the H^+ permeability barrier is also potentially important.

Claudin-8 is expressed along the aldosterone-sensitive distal nephron, including the entire collecting duct (Li *et al.* 2004). We propose that one of the major roles of claudin-8 is to form a barrier to prevent paracellular backleak of NH_4^+, HCO_3^- and H^+, thus playing a permissive role in urinary net acid excretion. The potential contribution of other claudin isoforms that are also expressed in the distal nephron and have cation barrier properties, such as claudin-4 (Van Itallie *et al.* 2001), is not yet known. Disturbances of claudin-8 function could potentially be the cause of distal renal tubular acidosis with a 'gradient'-type defect in which there are both H^+ and HCO_3^- leaks, as has been described (Zawadzki, 1998).

References

Adson A, Raub TJ, Burton PS, Barsuhn CL, Hilgers AR, Audus KL & Ho NF (1994). Quantitative approaches to delineate paracellular diffusion in cultured epithelial cell monolayers. *J Pharm Sci* **83**, 1529–1536.

Alexandre MD, Lu Q & Chen YH (2005). Overexpression of claudin-7 decreases the paracellular Cl^- conductance and increases the paracellular Na^+ conductance in LLC-PK1 cells. *J Cell Sci* **118**, 2683–2693.

Amasheh S, Meiri N, Gitter AH, Schoneberg T, Mankertz J, Schulzke JD & Fromm M (2002). Claudin-2 expression induces cation-selective channels in tight junctions of epithelial cells. *J Cell Sci* **115**, 4969–4976.

Batlle D & Flores G (1996). Underlying defects in distal renal tubular acidosis: New understandings. *Am J Kid Dis* **27**, 896–915.

Brewer ML, Schmitt UW & Voth GA (2001). The formation and dynamics of proton wires in channel environments. *Biophys J* **80**, 1691–1702.

Cereijido M (1984). Electrical properties of Madin-Darby canine kidney cells. *Fed Proc* **43**, 2230–2235.

Cereijido M, Robbins ES, Dolan WJ, Rotunno CA & Sabatini DD (1978). Polarized monolayers formed by epithelial cells on a permeable and translucent support. *J Cell Biol* **77**, 853–880.

Chernyshev A & Cukierman S (2002). Thermodynamic view of activation energies of proton transfer in various gramicidin A channels. *Biophys J* **82**, 182–192.

Colegio OR, Van Itallie CM, McCrea HJ, Rahner C & Anderson JM (2002). Claudins create charge-selective channels in the paracellular pathway between epithelial cells. *Am J Physiol Cell Physiol* **283**, C142–C147.

Dann RS & Koch GG (2005). Review and evaluation of methods for computing confidence intervals for the ratio of two proportions and considerations for non-inferiority clinical trials. *J Biopharm Stat* **15**, 85–107.

Decoursey TE (2003). Voltage-gated proton channels and other proton transfer pathways. *Physiol Rev* **83**, 475–579.

Flessner MF, Wall SM & Knepper MA (1991). Permeabilities of rat collecting duct segments to NH_3 and NH_4^+. *Am J Physiol* **260**, F264–F272.

Furuse M, Furuse K, Sasaki H & Tsukita S (2001). Conversion of zonulae occludentes from tight to leaky strand type by introducing claudin-2 into Madin-Darby canine kidney I cells. *J Cell Biol* **153**, 263–272.

Good DW, Caflisch CR & DuBose TD Jr (1987). Transepithelial ammonia concentration gradients in inner medulla of the rat. *Am J Physiol* **252**, F491–F500.

Graber ML, Bengele HH, Mroz E, Lechene C & Alexander EA (1981). Acute metabolic acidosis augments collecting duct acidification rate in the rat. *Am J Physiol* **241**, F669–F676.

Halm DR & Frizzell RA (1992). Anion permeation in an apical membrane chloride channel of a secretory epithelial cell. *J Gen Physiol* **99**, 339–366.

Hamm LL (2004). Renal acidification mechanisms. In *Brenner and Rector's the Kidney*, vol. I, ed. Brenner BM, pp. 497–534. Saunders, Philadelphia, PA, USA.

Hille B (2001). *Ionic Channels of Excitable Membranes*. Sinauer, Sunderland.

Ketchem R, Roux B & Cross T (1997). High-resolution polypeptide structure in a lamellar phase lipid environment from solid state NMR derived orientational constraints. *Structure* **5**, 1655–1669.

Kimizuka H & Koketsu K (1964). Ion transport through cell membrane. *J Theor Biol* **6**, 290–305.

Li WY, Huey CL & Yu AS (2004). Expression of claudin-7 and -8 along the mouse nephron. *Am J Physiol Renal Physiol* **286**, F1063–F1071.

Lide DR (2002). *CRC Handbook of Chemistry and Physics*. CRC Press, Boca Raton.

McCarthy KM, Francis SA, McCormack JM, Lai J, Rogers RA, Skare IB, Lynch RD & Schneeberger EE (2000). Inducible expression of claudin-1-myc but not occludin-VSV-G results in aberrant tight junction strand formation in MDCK cells. *J Cell Sci* **113**, 3387–3398.

Robinson RA & Stokes RH (1959). *Electrolyte Solutions*. Dover, Mineola, NY, USA.

Sansom MS, Kerr ID, Breed J & Sankararamakrishnan R (1996). Water in channel-like cavities: structure and dynamics. *Biophys J* **70**, 693–702.

Sasaki H, Matsui C, Furuse K, Mimori-Kiyosue Y, Furuse M & Tsukita S (2003). Dynamic behavior of paired claudin strands within apposing plasma membranes. *Proc Natl Acad Sci U S A* **100**, 3971–3976.

Schneeberger EE & Lynch RD (2004). The tight junction: a multifunctional complex. *Am J Physiol Cell Physiol* **286**, C1213–C1228.

Slater JC (1964). Atomic radii in crystals. *J Chem Phys* **41**, 3199–3204.

Tang VW & Goodenough DA (2003). Paracellular ion channel at the tight junction. *Biophys J* **84**, 1660–1673.

Tsukita S & Furuse M (2000). Pores in the wall: claudins constitute tight junction strands containing aqueous pores. *J Cell Biol* **149**, 13–16.

Van Itallie CM & Anderson JM (2004). The molecular physiology of tight junction pores. *Physiology (Bethesda)* **19**, 331–338.

Van Itallie C, Fanning AS & Anderson JM (2003). Reversal of charge selectivity in cation or anion selective epithelial lines by expression of different claudins. *Am J Physiol Renal Physiol* **285**, F1078–F1084.

Van Itallie C, Rahner C & Anderson JM (2001). Regulated expression of claudin-4 decreases paracellular conductance through a selective decrease in sodium permeability. *J Clin Invest* **107**, 1319–1327.

Yu AS, Enck AH, Lencer WI & Schneeberger EE (2003). Claudin-8 expression in MDCK cells augments the paracellular barrier to cation permeation. *J Biol Chem* **278**, 17350–17359.

Zawadzki J (1998). Permeability defect with bicarbonate leak as a mechanism of immune-related distal renal tubular acidosis. *Am J Kidney Dis* **31**, 527–532.

Acknowledgements

We thank Dr Horst Fischer (Children's Hospital, Oakland, CA, USA) for helpful suggestions. This work was supported in part by National Institutes of Health grants DK062283 (to A.S.L.Y.), HL038658 (to K.-J.K.) and HL064365 (to K.-J.K.).